ISSN (Print) 1226-1750
ISSN (Online) 2233-6656
Journal of Magnetics 28(2), 187-193 (2023) https://doi.org/10.4283/JMAG.2023.28.2.187

Electro-magnetic Visco-plastic Nanofluid Flow Considering Buongiorno Two-component Model in Frames of Darcy-Forchheimer Porosity, Transpiration and Joule Heating

Shuguang Li[1], M. Waqas[2,3], Salman A. AlQahtani[4]*, and M. Ijaz Khan[3,5]*

[1]*School of Computer Science and Technology, Shandong Technology and Business University, Yantai 264005, China*
[2]*NUTECH School of Applied Sciences and Humanities, National University of Technology, Islamabad, 44000, Pakistan*
[3]*Department of Mechanical Engineering, Lebanese American University, Beirut, Lebanon*
[4]*Department of Computer Engineering, College of Computer and Information Sciences, King Saud University, P.O. Box 51178. Riyadh 11543 Kingdom of Saudi Arabia*
[5]*Department of Mathematics and Statistics, Riphah International University I-14, Islamabad 44000, Pakistan*

(Received 1 May 2023, Received in final form 20 June 2023, Accepted 22 June 2023)

Enhancing heat transfer is of utmost importance in modern industrial applications. Pure liquids for illustration ethylene glycol, propylene glycol and water having lower conductivity are commonly used as cooling liquids in distinct applications. This approach helps conserve and optimize the enhancement of heat transportation. However, in order to achieve enhanced thermal efficiency, state-of-the-art liquids known as nanoliquids have been recommended. Thus the Buongiorno two-component nanoliquid model, which exhibits superior thermal efficiency compared to the aforementioned standard cooling liquids is being considered for formulating and analyzing the behavior of Casson nanoliquid configured by cylindrical convected surface. The problem formulation incorporates various factors such as Darcy-Forchheimer porosity, thermophoresis, magnetohydrodynamics, Brownian diffusion, suction/injection and Joule heating. Boundary-layer stretching flow is formulated. Dimensionless differential form from governing nonlinear problems is achieved by employing relevant variables. The application of the homotopy procedure results in convergent solutions for strongly nonlinear systems. The graphs are used to reveal the plots of significant factors in the analysis.

Keywords : buongiorno two-component model, darcy-forchheimer porosity, electro-magnetic characteristics, boundary-layer stretching flow, suction/injection.

1. Introduction

Nanotechnology refers to the field of science that focuses on comprehending the fundamental principles of materials science, biology, physics and chemistry at nanoscale [1]. The remarkable heat transportation performance exhibited by nanofluids [2, 3] containing nano-sized particles has garnered a significant consideration of modern researchers. A conventional heat-transferring fluid [4] can be transformed into a nanofluid by incorporating a lower concentration of nanowires, nanoparticles or nanotubes. The most frequently utilized types of elements are carbon-based nanoparticles, metal-oxide nanoparticles (including Al_2O_3, CuO, TiO_2) and metal nanoparticles (such as Au, Ag, Cu). Incorporating even a small quantity of solid particles into a nanofluid can significantly elevate its thermal conductivity [5] and enhance its heat transference coefficient during laminar flow [5, 6] in comparison to base fluid. The remarkable thermal properties of nanofluids have numerous potential applications in various heat transfer industries, such as electronics, engine cooling, energy systems, transformer oil, solar heating and heat exchange mechanisms [7]. The exceptional heat transference attributes of nanofluids are of significant interest to scientists, given their other remarkable characteristics. Modern researchers considered multi-physical assumptions to model fluid flow rheological problems based on nanofluids (see Refs. [8-16] and numerous investigations therein).

Scientists and engineers typically focus on working with fluids like oil, air and water which demonstrate

*Corresponding author: Tel: +92-300-9019713
e-mail: salmanq@ksu.edu.sa

Newtonian characteristics under diverse physical circumstances. In certain scenarios, relying solely on Newtonian models is unreliable and it becomes necessary to elaborate the fluids aspects elaborating non-Newtonian characteristics. Such situation frequently emerges in the industries of plastics manufacturing and chemical processing. Non-Newtonian characteristics can also be witnessed in mining industry, where the handling of muds along with slurries is a common occurrence. Additionally, this behavior is encountered in various other fields including pipeline industry, biomedical transport and tissue engineering. Consequently, the industry places great importance on simulating non-Newtonian flows. The recent advancements in biofluid dynamics and polymer manufacturing have sparked a growing interest in understanding the flow featuring non-Newtonian rheology via tubes subjected to a constant yield value. Among these fluids, the Casson fluid is commonly used. Casson fluids are liquids that unveil shear thinning behavior, meaning their viscosity declines with higher shear rate. They have infinite viscosity at zero shear rate and possess both zero yield stress and infinite shear rate. Currently, the Casson model is also being employed to develop rheological models for human blood. The literature (see Refs. [17-23]) provides detailed analyses of Casson fluid flow through various geometries under different conditions.

The current research focuses on examining the behavior of a convectively heated non-Newtonian viscoplastic (Casson) nanofluid subjected to thermal radiation. The analysis incorporates various factors such as Darcy-Forchheimer porosity, thermophoresis, magnetohydrodynamics, Brownian diffusion, suction/injection and Joule heating. Analytical procedure (homotopy analysis method [24-27]) is utilized to obtain convergent solutions for these highly nonlinear systems. The results are presented through graphs, revealing the influence of key parameters. Magneto-electric current [28], micro-channels transport [29], nano-based materials [30-32], heat transport [33, 34] are some recent and valuable research on different methodology and applications. Refs. [35-42] investigate some recent and new results in flow of fluid versus different flow assumptions.

2. Modeling

Consider a viscoplastic nanofluid which accelerate subjected to convectively heated stretchable permeable cylinder. Rheological features of Casson fluid are described considering incompressibility and steady-state situation. The problem is represented using a cylindrical coordinate system and Fig. 1, provides a visual depiction of the

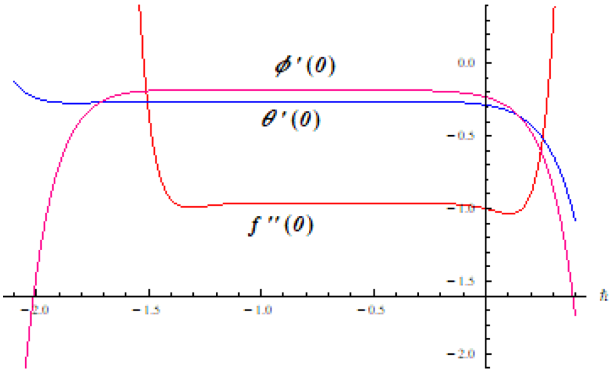

Fig. 1. (Color online) Combine $\hbar$-curves for momentum, temperature and concentration.

geometry. Modeling features multiphysical aspects such as Darcy-Forchheimer porosity, thermophoresis, magnetohydrodynamics, Brownian diffusion, suction/injection and Joule heating. The aforesaid assumptions correspond to following expressions:

$$\frac{\partial(ru)}{\partial x}+\frac{\partial(rv)}{\partial r}=0, \tag{1}$$

$$u\frac{\partial u}{\partial x}+v\frac{\partial u}{\partial r}=\nu\left(1+\frac{1}{\beta}\right)\left(\frac{\partial^2 u}{\partial r^2}+\frac{1}{r}\frac{\partial u}{\partial r}\right)-\frac{\sigma B_0^2}{\rho_f}u-\frac{\nu\Phi}{K^*}u\left(1+\frac{1}{\beta}\right)-\frac{C_b^*\Phi}{\sqrt{K^*}}u^2, \tag{2}$$

$$u\frac{\partial T}{\partial x}+v\frac{\partial T}{\partial r}=\frac{k}{(\rho c)_f}\left(\frac{\partial^2 T}{\partial r^2}+\frac{1}{r}\frac{\partial T}{\partial r}\right)+\tau\left(D_B\frac{\partial C}{\partial r}\frac{\partial T}{\partial r}+\frac{D_T}{T_\infty}\left(\frac{\partial T}{\partial r}\right)^2\right)$$
$$+\frac{16\sigma^* T_\infty^3}{3k^*(\rho c)_f}\left(\frac{\partial^2 T}{\partial r^2}+\frac{1}{r}\frac{\partial T}{\partial r}\right)+\frac{\sigma B_0^2 u^2}{(\rho c)_f}, \tag{3}$$

$$u\frac{\partial C}{\partial x}+v\frac{\partial C}{\partial r}=D_B\left(\frac{\partial^2 C}{\partial r^2}+\frac{1}{r}\frac{\partial C}{\partial r}\right)+\frac{D_T}{T_\infty}\left(\frac{\partial^2 T}{\partial r^2}+\frac{1}{r}\frac{\partial T}{\partial r}\right), \tag{4}$$

$$u=U_w=\frac{U_0 x}{l},\ v=-v_w,\ -k\frac{\partial T}{\partial r}=h_1\left(T_f-T\right),\ -D_B\frac{\partial C}{\partial r}=h_2\left(C_f-C\right)\ \text{at}\ r=R_1$$
$$u\to 0,\ T\to T_\infty(x),\ C\to C_\infty(x)\ \text{as}\ r\to\infty. \tag{5}$$

In the aforementioned Eqs. (1)-(5), velocity components (u, v) are in (x, r) directions respectively, l characteristic length, $\nu=\frac{\mu}{\rho_f}$ kinematic viscosity, β material parameter, μ dynamic viscosity, B_0 magnetic field potency, $\tau=\frac{(\rho c)_p}{(\rho c)_f}$ heat capacity ratio, ρ_f liquid density, (D_T, D_B) (thermophoretic, Brownian) diffusion, σ electrical conductivity of liquid, ($(\rho c)_f$, $(\rho c)_p$) (heat-capacity of liquid, nanoparticles effective heat-capacity), k^* coefficient of mean-absorption, (T_f, C_f) convective liquid (temperature, concentration), σ^* Stefan-Boltzmann constant, (U_w, U_0, v_w) (stretching, reference, suction/injection) velocity, (h_2, h_1) convective (mass, heat) transference coefficients and (T_∞, C_∞)

ambient liquid (temperature, concentration).

Employing

$$\eta=\sqrt{\frac{U_w}{\nu x}}\left(\frac{r^2-R_1^2}{2R_1}\right),\ \psi=\sqrt{U_w\nu x}R_1 f(\eta),\ \theta(\eta)=\frac{T-T_\infty}{T_f-T_\infty},$$
$$\phi(\eta)=\frac{C-C_\infty}{C_f-C_\infty},\ u=U_w f'(\eta),\ v=\sqrt{\frac{\nu U_0}{l}}\frac{R_1}{r}f(\eta), \tag{6}$$

continuity equation (i.e., Eq. (1)) is satisfied trivially while Eqs. (2)-(6) yield:

$$\begin{aligned}&(1+2\gamma\eta)\left(1+\frac{1}{\beta}\right)f'''+2\gamma f''+ff''-f'^2-\beta_1\left(1+\frac{1}{\beta}\right)f'\\&-\beta_2 f'^2-Ha^2 f'=0,\end{aligned} \tag{7}$$

$$\left.\begin{aligned}&(1+2\gamma\eta)\left(1+\frac{4}{3}R\right)\theta''+2\gamma\left(1+\frac{4}{3}R\right)\theta'+\Pr f\theta'\\&+\Pr(1+2\gamma\eta)\left(N_b\theta'\phi'+N_t\theta'^2\right)+\Pr EcHa^2 f'^2=0,\end{aligned}\right\} \tag{8}$$

$$(1+2\gamma\eta)\phi''+2\gamma\phi'+Scf\phi'+\frac{N_t}{N_b}\left((1+2\gamma\eta)\theta''+2\gamma\theta'\right)=0, \tag{9}$$

$$\left.\begin{aligned}&f=S,\ f'=1,\ \theta'(0)=-\gamma_1(1-\theta(\eta)),\\&\phi'(0)=-\gamma_2(1-\phi(\eta))\ \text{at}\ \eta=0,\\&f'\to 0,\ \theta\to 0,\ \phi\to 0\ \text{as}\ \eta\to\infty.\end{aligned}\right\} \tag{10}$$

In Eqs. (7)-(10), $\gamma=\sqrt{\frac{\nu l}{u_0 R_1^2}}$ illustrates curvature parameter, $\beta_1=\frac{\nu\Phi}{cK^*}$ the inertia variable, $\Pr=\frac{\mu c_p}{k}$ Prandtl number, $\beta_2=\frac{C_b^*\Phi}{\sqrt{K^*}}$ Darcy porosity variable, $N_t=\frac{\tau D_T(T_f-T_\infty)}{\alpha T_\infty}$ thermophoretic factor, $R=\frac{4\sigma^* T_\infty^3}{kk^*}$ radiation variable, $N_b=\frac{\tau D_B(C_f-C_\infty)}{\alpha}$ Brownian diffusion factor, $S=v_w\sqrt{\frac{l}{U_0\nu}}$ (suction ($S>0$), injection ($S<0$) parameter, $\left(\gamma_2=\frac{h_2}{D_B}\sqrt{\frac{\nu l}{U_0}},\ \gamma_1=\frac{h_1}{k}\sqrt{\frac{\nu l}{U_0}},\right)$ (solutal, thermal) Biot numbers, $Ha=\frac{\sigma B_0^2 l}{\rho U_0}$ Hartman number and $Ec=\frac{U_w^2}{c_f(T_f-T_\infty)}$ Eckert number.

The mathematical forms of drag force (C_{fx}) together with heat-mass transference rates (Nu_x, Sh_x) are expressed as:

$$C_f=\frac{\tau_w}{\rho_f U_w^2},\ \tau_w=\left[\mu\left(1+\frac{1}{\beta}\right)\left(\frac{\partial u}{\partial r}\right)\right]_{r=R_1}, \tag{11}$$

$$Nu_x=\frac{xq_w}{k(T_f-T_\infty)},\ q_w=-k\left(\frac{\partial T}{\partial r}\right)_{r=R_1}-\frac{16\sigma^* T_\infty^3}{3k^*}\left(\frac{\partial T}{\partial r}\right)_{r=R_1}, \tag{12}$$

$$Sh_x=\frac{xq_m}{D_B(C_f-C_\infty)},\ q_m=-D_B\left(\frac{\partial C}{\partial r}\right)_{r=R_1}. \tag{13}$$

Eqs. (11)-(13) in dimensionless forms yield:

$$C_{f_x}\,\mathrm{Re}_x^{1/2}=\left(1+\frac{1}{\beta}\right)f''(0), \tag{14}$$

$$Nu_x\,\mathrm{Re}_x^{-1/2}=-\left(1+\frac{4}{3}R\right)\theta'(0), \tag{15}$$

$$Sh_x\,\mathrm{Re}_x^{-1/2}=-\phi'(0), \tag{16}$$

in which Reynolds number is denoted by $\mathrm{Re}_x=lU_w/\nu$.

3. Computational Analytical Scheme

This section features analytical solutions obtained through homotopic algorithm [24-27]. This algorithm requires base-functions $(f_0(\eta),\ \theta_0(\eta),\ \phi_0(\eta))$ together with operators $(L_f,\ L_\theta,\ L_\phi)$ in the forms given below:

$$\begin{aligned}&f_0(\eta)=S+(1-e^{-\eta}),\\&\theta_0(\eta)=\frac{\gamma_1\exp(-\eta)}{1+\gamma_1},\\&\phi_0(\eta)=\frac{\gamma_2\exp(-\eta)}{1+\gamma_2},\end{aligned} \tag{17}$$

$$\begin{aligned}&L_f=f'''-f',\\&L_\theta=\theta''-\theta,\\&L_\phi=\phi''-\phi.\end{aligned} \tag{18}$$

The operators mentioned above obey:

$$\begin{aligned}&L_f(C_1+C_2e^{\eta}+C_3e^{-\eta})=0,\\&L_\theta(C_6e^{\eta}+C_7e^{-\eta})=0,\\&L_\phi(C_8e^{\eta}+C_9e^{-\eta})=0,\end{aligned} \tag{19}$$

where C_i (i = 1-9) signify arbitrary constants.

4. Convergence

No doubt the utilization of homotopic algorithm yields series solutions which may converge or diverge. One has to ensure the convergence of obtained results while using homotopic algorithm. To achieve this, an assisting factor $(\hbar)$ is utilized to adjust and monitor the convergence region of obtained series solutions. By analyzing the $\hbar$ -curves depicted in Fig. 2, optimized estimations for $\hbar_f, \hbar_\theta$ and $\hbar_\phi$ are $-1.25\le\hbar_f\le-0.30$, $-1.8\le\hbar_\theta\le-0.25$ and $-1.65\le\hbar_\phi\le-0.26$ respectively. These ranges of $\hbar_f, \hbar_\theta$ and $\hbar_\phi$ are attained at 12th order approximations. Numerical analysis, as shown in Table 1, also confirms the convergence arithmetically. It is evident that Eqs. (7)-(9) converge at 13th order approximations. Besides the

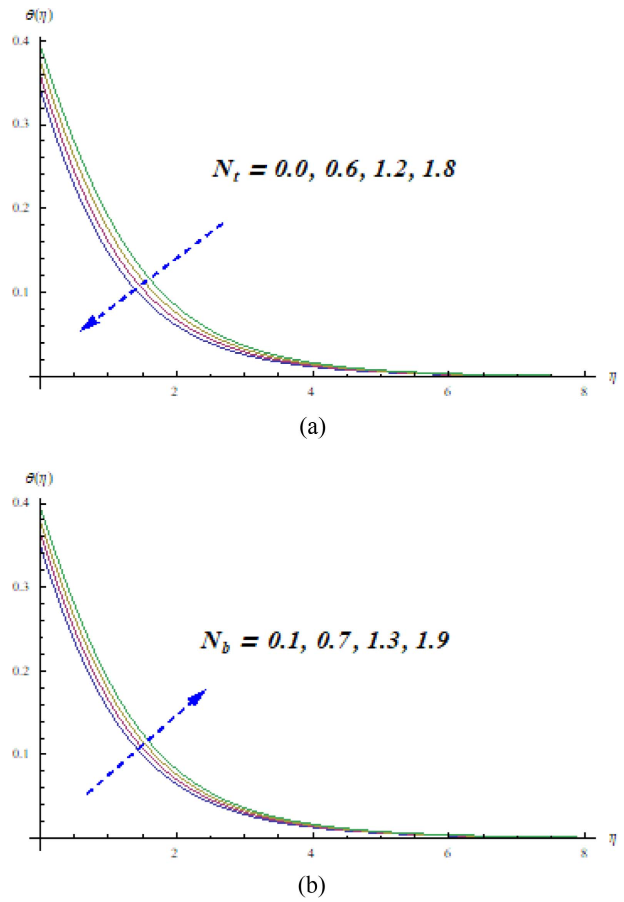

Fig. 2. (Color online) (a). *Nt* variations against temperature, (b) N_b variations against temperature.

Table 1. Convergence outcomes at different deformations order considering $\gamma = N_t = \beta_1 = N_b = \beta_2 = 0.1$, $Ha = R = 0.2$, $S = \gamma_2 = Ec = 0.3$, $\gamma_1 = 0.4$, $\Pr = Sc = 1.1$ and $\beta = 1.5$.

Approximations order	$-f''(0)$	$-\theta'(0)$	$-\phi'(0)$
1	0.9850	0.2753	0.2132
5	0.9644	0.2617	0.1889
10	0.9633	0.2593	0.1828
15	0.9630	0.2589	0.1817
20	0.9630	0.2589	0.1817
25	0.9630	0.2589	0.1817
30	0.9630	0.2589	0.1817

parametric values are selected arbitrarily as $\gamma = N_t = \beta_1 = N_b = \beta_2 = 0.1$, $Ha = R = 0.2$, $S = \gamma_2 = Ec = 0.3$, $\gamma_1 = 0.4$, $\Pr = Sc = 1.1$ and $\beta = 1.5$.

Figs. 2 and 3 elaborate the temperature response when nanoscale factors, specifically thermophoresis (N_t) and Brownian movement (N_b) are varied independently. A noticeable increase in temperature is found subjected to increasing N_t and N_b. The expression of thermophoretic body force (i.e., $N_t\theta'^2$) occurring in Eq. (8) is strengthened when the thermophoresis parameter N_t increases. The presence of a higher N_t values (see Fig. 2a) assists in the movement of nanoparticles in the presence of a larger temperature gradient. This leads to an elevation in the thermophoretic term, which in turn, upsurges the viscosity of the thermal boundary-layer on cylindrical sensor. Besides, from Fig. 2b, it is scrutinized that higher N_b estimations corresponds to nanoparticles with smaller diameters. This leads to more frequent and energetic collisions between the nanoparticles, resulting in intensified chaotic motions and subsequently elevated temperatures. Larger N_b signifies that the Brownian motion factor N_b appearing in Eq. (8) through the term $N_b\theta'\phi'$ is amplified, resulting in an energized regime. This enhancement in Brownian motion factor (N_b) promotes heat transfers by increasing the thickness of thermal boundary-layer. Consequently, this confirms the heat enhancement aspects achieved through the utilization of nanofluids. Fig. 3a demonstrates that increasing Eckert number (*Ec*) corresponds to higher temperature. This augmentation indicates the

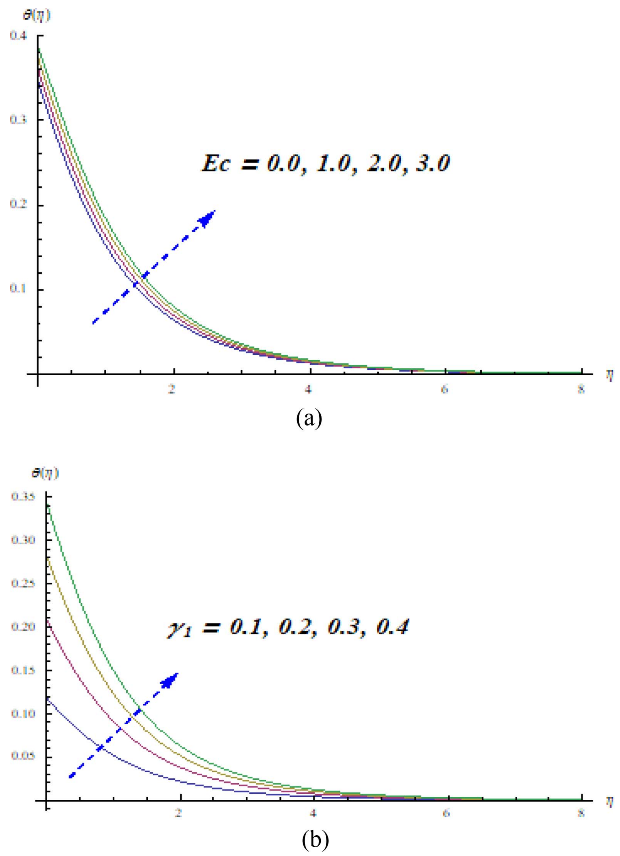

Fig. 3. (Color online) (a) *Ec* variations against temperature, (b) γ_1 variations against temperature.

presence of viscous heating effects within the nano-polymer. The importance of viscous heating should not be ignored, predominantly considering its impact in dynamics of polymer coatings. The Eckert number $Ec = \frac{U_w^2}{c_f(T_f - T_\infty)}$ represents the relation of kinetic energy dissipated in the flow to enthalpy difference in the boundary-layer. Note that $Ec > 0$, heat transfers away from cylindrical surface towards the boundary-layer. Neglecting this effect in thermally magnetized nano-coating based models would result in underestimating temperatures in the boundary layer and less accurate characterization of thermal distribution. Analysis of Fig. 3b indicates a substantial increase in temperature when γ_1 upsurges. As γ_1 upsurges, there is an enhanced heat transportation from wall towards boundary-layer, which is a progressive effect. This encourages thermo diffusion in the nano-polymer and leads to a heating aspect, resulting in a thicker thermal boundary-layer.

Fig. 4a reveals that higher N_t counteracts the impact of Brownian movement (N_b). There is a significant intensification in nano-particle concentrations, resulting in an elevated thickness of species boundary-layer. Clearly N_t and N_b occur in energy Eq. (8) via terms $N_b\theta'\phi' + N_t\theta'^2$ while they also emerge in Eq. (9) through the term $\frac{N_t}{N_b}\left(\left(1+2\gamma\eta\right)\theta''\right)$. Thermophoresis promotes the migration of particles from hotter to colder zones and aids in species diffusion, leading to an increase in the thickness of concentration boundary-layer (see Fig. 4a). On the other hand, Brownian movement disperses nanoparticle distribution because of chaotic motion resulting from flow

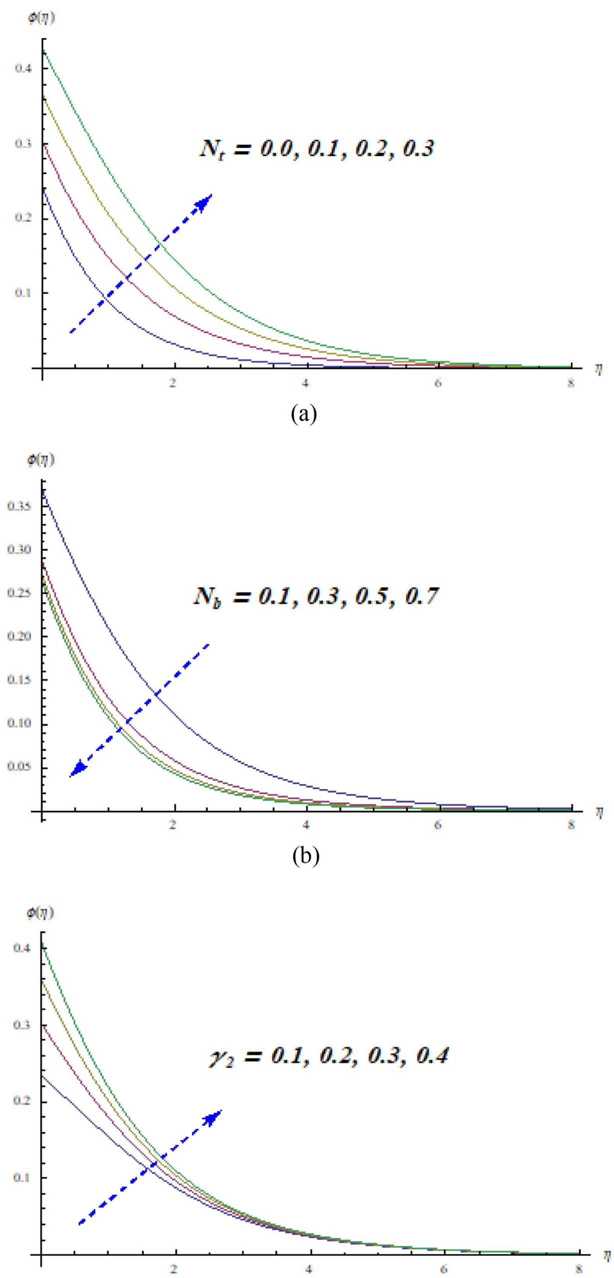

Fig. 4. (Color online) (a) N_t variations against concentration, (b) N_b variations against concentration, γ_2 variations against concentration.

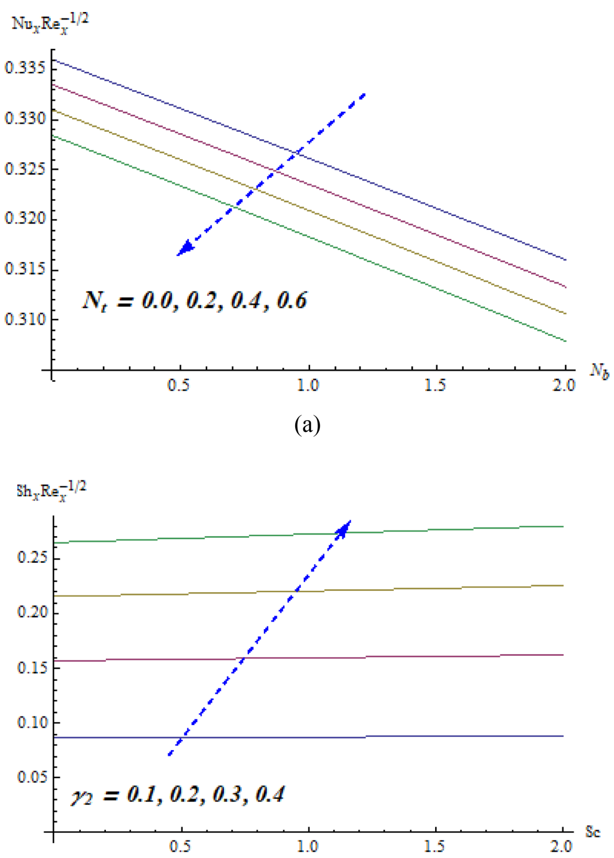

Fig. 5. (Color online) (a) *Nt* and *Nb* variations against Nusselt number, (b) γ_2 and *Sc* variations against Sherwood number.

acceleration, thereby reducing the thickness of concentration boundary-layer (see Fig. 4b). The increase in solutal Biot number (γ_2), as computed in Fig. 4c has a pronounced effect of elevating nano-particles concentration $\left(\phi(\eta)\right)$, where $\phi(\eta)$ is an increasing function of γ_2. As a result, there is a substantial enhancement in the thickness of concentration boundary-layer accompanying the escalation in γ_2.

The heat transportation rate (i.e., local Nusselt number $\left(Nu_x \operatorname{Re}_x^{-1/2}\right)$ is reduced with an increase in N_t and N_b since these nanoscale effects aid in heating boundary-layer and diminish thermal transportation to wall (see Fig. 5a). Consequently, heat transportation rates can be effectively controlled by precisely selecting these thermo-physical factors. On the other hand, a reverse situation is witnessed against mass transportation rate (i.e., local Sherwood number $\left(Sh_x \operatorname{Re}_x^{-1/2}\right)$ when γ_2 and Sc are augmented.

5. Conclusions

A mathematical and theoretical study featuring magnetization impact in viscoplastic non-Newtonian Casson model utilizing two-component Buongiorno's model is presented. The analysis incorporates various factors such as Darcy-Forchheimer porosity, thermophoresis, magneto-hydrodynamics, Brownian diffusion, suction/injection and Joule heating. This simulation aimed to simulate the processing of higher temperature based nano-polymeric materials. The main outcomes extracted from the presented simulations are stated below:

- Increasing thermophoresis (N_t) and Brownian movement (N_b) tend to upsurge the nanofluid temperature distribution. On the other hand, heat transportation rate is reduced with an increase in N_t and N_b.
- Enlarging Eckert number and thermal Biot number enhance temperature.
- Nanoparticles species concentration is significantly reduced for increasing estimations of Brownian motion while it discloses reverse influence nanoparticles species concentration for thermophoresis factor.
- Enhancing estimations of solutal Biot number significantly upsurge the nanoparticles concentration and mass transportation.

The elaborated research has shown the impressive effectiveness of HAM in simulating the dynamic flow of nonlinear thermally magnetized nano-polymeric coatings. However, the focus has been primarily on the Darcy-Forchheimer porosity model. In future researches, more sophisticated non-Newtonian models featuring accurate Darcy-Forchheimer porosity term will be explored, and the findings will be communicated soon.

Acknowledgement

This Research is funded by Research Supporting Project Number (RSPD2023R585, King Saud University, Riyadh, Saudi Arabia.

References

[1] J. A. Ali, K. Kolo, A. K. Manshad, and A. H. Mohammadi, Egyptian Journal of Petroleum **27**, 1371 (2018).
[2] J. A. Eastman, S. U. S. Choi, S. Li, W. Yu, and L. J. Thompson, Applied Physics Letters **78**, 718 (2001).
[3] J. A. Eastman, S. R. Phillpot, S. U. S. Choi, and P. Keblinski, Annual Review of Materials Research **34**, 219 (2004).
[4] Y. Xuan and Q. Li, International Journal of Heat and Fluid Flow **21**, 58 (2000).
[5] S. K. Das, N. Putra, P. Thiesen, and W. Roetzel, ASME Journal of Heat Transfer **125**, 567 (2003).
[6] Y. Xuan and Q. Li, ASME Journal of Heat Transfer **125**, 151 (2003).
[7] R. Saidur, K. Y. Leong, and H. A. Mohammed, Renewable and Sustainable Energy Reviews **15**, 1646 (2011).
[8] A. B. Jafar, S. Shafie, and I. Ullah, Heliyon **6**, e04201 (2020).
[9] A. A. A. Arani and H. Aberoumand, Powder Technology **380**, 152 (2021).
[10] A. M. Sedki, Results in Materials **16**, 100334 (2022).
[11] A. Mathew, S. Areekara, and A. S. Sabu, Journal of the Indian Chemical Society **99**, 100615 (2022).
[12] M. Nasir, M. Waqas, O. A. Bég, H. F. M. Ameen, N. Zamri, K. Guedri, and S. M. Eldin, , Micromachines **13**, 2196 (2022).
[13] Y. M. Chu, S. Jakeer, S. R. R. Reddy, M. L. Rupa, Y. Trabelsi, M. I. Khan, H. A. Hejazi, B. M. Makhdoum, and S. M. Eldin, Case Studies in Thermal Engineering **44**, 102838 (2023).
[14] F. Wang, M. Waqas, W. A. Khan, B. M. Makhdoum, and S. M. Eldin, Computational Particle Mechanics, DOI: 10.1007/s40571-023-00579-w (2023).
[15] Y. Masthanaiah, N. Tarakaramu, M. I. Khan, A. Rushikesava, S. B. Moussa, B. M. Fadhl, S. S. Abdullaev, and S. M. Eldin, Case Studies in Thermal Engineering **47**, 103059 (2023).
[16] A. S. Abdelrazik, M. A. M. Sayed, A. M. A. Omar, A. F. M. Fatma, H. E. Alshimaa, A. Oulguidoum, E. Kotob, and M. H. M. Helmy, Journal of Molecular Liquids **381**, 121757 (2023).
[17] N. Casson, Rheology of disperse systems, 1959.
[18] M. I. Khan, M. Waqas, T. Hayat, and A. Alsaedi, Journal of Colloid and Interface Science **498**, 85 (2017).
[19] A. S. Oke , W. N. Mutuku, M. Kimathi, and I. L. Anima-

saun, Nonlinear Engineering **9**, 398 (2020).
[20] N. C. Roy and G. Saha, Arabian Journal for Science and Engineering **47**, 16091 (2022).
[21] M. Nasir, M. Waqas, N. Zamri, N. B. Khedher, and K. Guedri, Computational Particle Mechanics, https://doi.org/10.1007/s40571-022-00547-w (2023).
[22] Q. Khan, M. Farooq, and S. Ahmad, Ain Shams Engineering Journal https://doi.org/10.1016/j.asej.2023.102253 (2023).
[23] P. Vaidehi and J. Sasikumar, Thermal Science and Engineering Progress **42**, 101885 (2023).
[24] S. J. Liao, Springer, Heidelberg, Germany, (2012).
[25] S. Khan , M. M. Selim, K. A. Gepreel, A. Ullah, Ikramullah, M. Ayaz, W. K. Mashwani, and E. Khan, Open Physics **19**, 341 (2021).
[26] K. A. Khan, A. R. Seadawy, and N. Raza, Chaos, Solitons & Fractals **157**, 111888 (2022).
[27] M. Yasir, M. Khan, and Z. U. Malik, International Communications in Heat and Mass Transfer **141**, 106577 (2023).
[28] C. Lu, H. Zhou, L. Li, A. Yang, C. Xu, Z. Ou, ...F. Tian, Journal of the International Measurement Confederation **188**, 110527 (2022).
[29] Z. Gao, S. Hong, and C. Dang, Applied Thermal Engineering **226**, 120283 (2023).
[30] Y. Zhang, G. Liu, J. Ye, and Y. Lin, Composite Structures **299,** 116087 (2022).
[31] X. Zhang, Y. Tang, F. Zhang, and C. Lee, Advanced Energy Materials **6,** 1502588 (2016).
[32] N. Sun, X. Yao, J. Liu, J. Li, N. Yang, G. Zhao, ….., and C. Dai, Geoenergy Science and Engineering **223**, 211513 (2023).
[33] Z. Y. Zhu, Y. L. Liu, G. Q. Gou, W. Gao, and J. Chen, Scientific Reports **11**, 10020 (2021).
[34] Q. Zhu, J. Chen, G. Gou, H. Chen, and P. Li, Journal of Materials Processing Technology **246**, 267 (2017).
[35] M. F. Ahmed, A. Zaib, F. Ali, O. T. Bafakeeh, E. S. M. Tag-ElDin, K. Guedri, S. Elattar, and M. I. Khan, Micromachines **13**, 1768 (2022).
[36] R. N. Kumar, R. J. P. Gowda, J. K. Madhukesh, B. C. Prasannakumara, and G. K. Ramesh, Physica Scripta **96**, 075210 (2021).
[37] O. T. Bafakeeh, K. Raghunath, F. Ali, M. Khalid, E. S. M. Tag-ElDin, M. Oreijah, K. Guedri, N. B. Khedher, and M. I. Khan, Catalysts **12**, 1233 (2022).
[38] R. S. V. Kumar, A. Alhadhrami, R. J. P. Gowda, R. N. Kumar, and B. C. Prasannakumara, ZAMM - Journal of Applied Mathematics and Mechanics **101**, e202100035 (2021).
[39] N. Manzoor, I. Qasim, M. I. Khan, M. W. Ahmed, K. Guedri, O. T. Bafakeeh, E. S. M. Tag-Eldin, and A. M. Galal, Applied Sciences **12**, 9737 (2022).
[40] R. J. P. Gowda, R. N. Kumar, A. M. Jyothi, B. C. Prasannakumara, and K. S. Nisar, ZAMM - Journal of Applied Mathematics and Mechanics **101**, e202000372 (2021).
[41] M. Shahid, H. M. A. Javed, M. I. Ahmad, A. A. Qureshi, M. I. Khan, M. A. Alnuwaiser, A. Ahmed, M. A. Khan, E. S. M. Tag-ElDin, A. Shahid, and A. Rafique, Nanomaterials, **12**, 3413 (2022).
[42] B. Mahanthesh, B. J. Gireesha, B. C. Prasannakumara, and P. B. S. Kumar, Results in Physics **7**, 2990 (2017).